

# Geophysical Research Letters

## RESEARCH LETTER

10.1029/2020GL091836

### Key Points:

- Constrain a microphysics scheme using new cloud and drizzle retrievals
- Implemented the updated scheme in National Center for Atmospheric Research Community Earth System Model to simulate the warm rain globally
- New scheme alleviates a long-lasting problem in most climate models

### Supporting Information:

- Supporting Information S1

### Correspondence to:

X. Dong,  
[xdong@arizona.edu](mailto:xdong@arizona.edu)

### Citation:

Dong, X., Wu, P., Wang, Y., Xi, B., & Huang, Y. (2021). New observational constraints on warm rain processes and their climate implications. *Geophysical Research Letters*, 48, e2020GL091836. <https://doi.org/10.1029/2020GL091836>

Received 24 NOV 2020

Accepted 4 MAR 2021

## New Observational Constraints on Warm Rain Processes and Their Climate Implications

Xiquan Dong<sup>1</sup> , Peng Wu<sup>1</sup> , Yuan Wang<sup>2,3</sup> , Baike Xi<sup>1</sup> , and Yiyi Huang<sup>1</sup> 

<sup>1</sup>Department of Hydrology and Atmospheric Sciences, University of Arizona, Tucson, AZ, USA, <sup>2</sup>Division of Geological and Planetary Sciences, California Institute of Technology, Pasadena, CA, USA, <sup>3</sup>Jet Propulsion Laboratory, California Institute of Technology, Pasadena, CA, USA

**Abstract** Low stratiform clouds have profound impacts on the hydrological cycle and the Earth's radiation budget. However, realistic simulation of low clouds in climate models presents a major challenge. Here we employ the newly retrieved cloud and drizzle microphysical properties to improve the autoconversion and accretion parameterizations in a microphysical scheme. We find that the new autoconversion (accretion) rate contributes 14% lower (greater) to total drizzle water content than the original scheme near the cloud top. Compared to satellite results, the simulated cloud liquid water path (LWP) and shortwave cloud radiative effect using the original scheme in a climate model agree well on global average but with large regional differences. Simulations using the updated scheme show a 7.3% decrease in the light rain frequency, and a 10% increase in LWP. The updated microphysics scheme alleviates the long-lasting problem in most climate models, that is “too frequent and too light precipitation.”

**Plain Language Summary** There has been a growing concern that most climate models predict too frequent and too light precipitation, which is primarily due to lack of reliable sub-grid variability and vertical variations of microphysical processes in low clouds. With the newly retrieved cloud and drizzle microphysical properties from a recent field campaign, we updated the classic warm rain microphysical scheme which was developed by Khairoutdinov and Kogan (2000, [https://doi.org/10.1175/1520-0493\(2000\)128<0229:ANCPPI>2.0.CO;2](https://doi.org/10.1175/1520-0493(2000)128<0229:ANCPPI>2.0.CO;2)) and widely used in weather and climate models. We examined relative contributions of different microphysical processes to the rain drop formation and growth processes. The altered scheme reflects the advance in process-level understanding of warm rain processes and reveals their relative contributions to the rain drop formation and growth processes at different cloud heights. The altered scheme has the potential of mitigating the long-lasting problem in most climate models and achieving more accurate climate assessments. Our findings unambiguously attest the paramount importance of cloud microphysical parameterizations in climate simulation.

## 1. Introduction

Low-level stratiform clouds (hereafter called low clouds) have been a topic of considerable interest because they strongly reflect incoming shortwave radiation (Stephens et al., 2015) and exert complex feedbacks on the climate system (Hang et al., 2019; IPCC, 2013; L'Ecuyer et al., 2019; Stephens, 2005; Wood, 2012). The radiative effect of low clouds contributes to one of the largest uncertainties in climate modeling (IPCC, 2013; Stephens et al., 2015) and has been well known to be influenced by aerosols (Fan et al., 2016; Ghan et al., 2016; Li et al., 2020; Penner et al., 2004; Seinfeld et al., 2016). Drizzle is common in maritime low clouds (Dong, Xi, Kennedy et al., 2014; Dong, Xi, & Wu, 2014; Wu et al., 2015). The formation of drizzle significantly modulates stratocumulus-to-cumulus transition (Yamaguchi et al., 2017) and plays an important role in determining cloud lifetime (Albrecht, 1989). Furthermore, they have profound impacts on the hydrological cycle and the Earth's radiation budget (Kay et al., 2018; Stephens et al., 2010, 2015; Suzuki et al., 2010; Wood et al., 2009), and consequently on the Earth's climate (Bony et al., 2005; Schmidt et al., 2006). Despite their importance, it is challenging to simulate low clouds realistically in climate models where they disagree substantially in the magnitude of cloud feedback for the regimes of low clouds. As a result, most general circulation models (GCMs) predict too frequent and too light precipitation (Donner et al., 2011;

Jing et al., 2017, 2018; Lebsock et al., 2013; Soden et al., 2011; Stephens et al., 2010; Wu et al., 2018; Zhang et al., 2019).

Another great challenge in GCMs is how to evaluate the cloud microphysical processes, such as autoconversion ( $R_{auto}$ ) and accretion ( $R_{accr}$ ) rates in low clouds (Wu et al., 2018; Zhang et al., 2019) since these processes cannot be directly measured. In fact, these processes are often parameterized as power law relationships with cloud and drizzle properties in model simulations. Satellite results have been widely used to evaluate these processes and concluded that GCM simulations are very sensitive to the choices of threshold cloud droplet radius in simulating the cloud-to-rain particle (Nakajima et al., 2010; Suzuki et al., 2010, 2013, 2015;). However, satellite retrievals suffer relatively large uncertainties, originating from their measurement and retrieval errors, as well as their limitations in observing clouds, especially for drizzling clouds (Ma et al., 2018; Suzuki et al., 2010). Most GCMs predict too frequent and too light precipitation due to lack of reliable sub-grid variability and vertical variations of  $R_{auto}$  and  $R_{accr}$  (Cheng & Xu, 2009; Golaz et al., 2002; Jing et al., 2017; Liu et al., 2007; Suzuki et al., 2010; Wood & Hartmann, 2006; Wu et al., 2018; Zhang et al., 2019).

The retrieved cloud and drizzle microphysical properties during the Aerosol and Cloud Experiments in the Eastern North Atlantic (ACE-ENA) field campaign (Wu et al., 2020) have 1-min temporal and 30-m vertical resolution, which are important for studying warm rain processes. In this study, we used the retrievals to recalibrate the  $R_{auto}$  and  $R_{accr}$  parameterizations in Khairoutdinov and Kogan (2000) scheme (hereafter called KK) into the new KK scheme (hereafter called NKK). The profiles of  $R_{auto}$  and  $R_{accr}$  ( $R_{auto}(Z)$  and  $R_{accr}(Z)$ , where  $Z$  is the in-cloud height) can be used to advance the process-level understanding of warm rain process. To further test the NKK scheme, we implemented the  $R_{auto}(Z)$  and  $R_{accr}(Z)$  into the National Center for Atmospheric Research (NCAR) Community Earth System Model (CESM, Hurrell et al., 2013; Morrison & Gettelman, 2008; Gettelman et al., 2019) to simulate the warm rain frequency and intensity globally.

## 2. Methods

### 2.1. Recalibrate the KK Warm Rain Scheme

A brief summary about the ground-based retrieval (Wu et al., 2020) is presented in the Supporting Information. The retrieved microphysics include cloud-droplet (drizzle) number concentration  $N_c$  ( $N_d(Z)$ ) liquid water content  $LWC_c(Z)$  ( $LWC_d(Z)$ ) and mass weighted mean radius  $r_c(Z)$  ( $= \left( \frac{3LWC_c}{4N_c\pi\rho_w} \right)^{1/3}$ ) and  $r_d(Z)$ . The units of  $LWC$ ,  $r$ , and  $N$  in this study are  $\text{gm}^{-3}$ ,  $\mu\text{m}$ , and  $\text{cm}^{-3}$ , respectively. Figures S1a–S1d show the retrieved cloud and drizzle microphysical properties. The retrieved  $LWC_c(Z)$  and  $r_c(Z)$  increased from the cloud base, peaked just below the cloud top, and then decreased toward the cloud top. The retrieved  $r_d(Z)$  and  $LWC_d(Z)$  (Figures S1c and S1d), opposite to their cloud counterparts, increased from the cloud top downward, peaked in the middle or bottom of the cloud, and decreased further down.

The  $R_{auto}$  and  $R_{accr}$  are usually parameterized as power law relationships with cloud and rain water mixing ratios ( $q_c$  and  $q_r$ ) and  $N_c$  (KK; Beheng, 1994; Kessler, 1969; Liu & Daum, 2004; Tripoli et al., 1980), and in the forms of

$$R_{auto}(Z) = \left( \frac{\partial q_r}{\partial t} \right)_{auto} = A q_c^{a1}(Z) N_c^{a2}, \quad (1)$$

$$R_{accr}(Z) = \left( \frac{\partial q_r}{\partial t} \right)_{accr} = B \left( q_c(Z) q_r(Z) \right)^b, \quad (2)$$

where  $A$ ,  $a1$ ,  $a2$ ,  $B$ , and  $b$  are coefficients in different schemes and are usually constants. In this study,  $q_c(Z)$  and  $q_r(Z)$  can be calculated from retrieved  $LWC_c(Z)$  and  $LWC_d(Z)$  and dry air density ( $\rho_{air}$ ), therefore,  $R_{auto}(Z)$  and  $R_{accr}(Z)$  are a function of height  $Z$  in Equations 1 and 2. In addition to  $LWC_c(Z)$  and  $LWC_d(Z)$ , the retrieved layer-mean  $N_c$  is also used in Equation 1. As a proof of concept, the KK scheme is used as an example in this study, in which  $A = 1,350$ ,  $a1 = 2.47$ ,  $a2 = -1.79$ ,  $B = 67$ , and  $b = 1.15$ .

The summation of  $R_{auto}(Z)$  and  $R_{accr}(Z)$  is the total drizzle water production rate ( $P_r(Z)$ ), which can be converted to  $LWC_d(KK)$  ( $= \int \rho_{air} P_r(Z) * dt$ ,  $dt$  is 1 min here) to directly compare with retrieved  $LWC_d(Z)$  with 1-min temporal resolution. The retrieved  $LWC_d(Z)$  is then used to scale the time interval of  $LWC_d(KK)$  within 1 min as

$$R'_{auto}(Z) = \frac{LWC_d(Z)}{\int \rho_{air} P_r(Z) dt} R_{auto}(Z) = A'(Z) q_c^{2.47}(Z) N_c^{-1.79}, \quad (3)$$

$$R'_{accr}(Z) = \frac{LWC_d(Z)}{\int \rho_{air} P_r(Z) dt} R_{accr}(Z) = B'(Z) (q_c(Z) q_r(Z))^{1.15}. \quad (4)$$

$A'(Z)$  and  $B'(Z)$ , which are functions of height  $Z$  with unitless, can be calculated from Equations 3 and 4. To clarify the terms used in this study,  $R_{auto}(Z)$  and  $R_{accr}(Z)$ , and constants  $A$  and  $B$  are used in KK scheme, while  $R'_{auto}(Z)$  and  $R'_{accr}(Z)$ , and  $A'(Z)$  and  $B'(Z)$  are used in NKK scheme.

A sensitivity study has shown that the coefficients  $A$  and  $B$  in Equations 1 and 2 are more or less dependent on the retrieved  $r_c$  and  $r_d$  than other coefficients  $a1$ ,  $a2$ , and  $b$ . Also, because of the linear constraining in Equations 3 and 4, the linear coefficients  $A$  and  $B$  are modified in this study and the exponential terms are retained. The relationship between  $q_c$  and  $N_c$  in KK does constrain  $r_c$ , but this constraint seems too weak in the lower part of cloud and too strong in the upper (Figure S1f).

The  $LWC_d(KK)$  profiles peaked in the center and upper part of the cloud (Figure S1e), which are different from the retrieved  $LWC_d(ret)$ . The ratios of  $LWC_d(KK)$  to  $LWC_d(ret)$  (Figure S1f) show that  $LWC_d(KK)$  were overestimated in the upper part and underestimated in the lower part of the cloud. The higher  $LWC_d$  ratios in the upper part and reduced ratios in the lower part of the cloud suggest that it is imperative to recalibrate and constrain the KK scheme using observations. The profiles of the  $LWC_d$  ratios in Figure S1f motivate us to modify the coefficients  $A$  and  $B$  as a function of height  $Z$ , such as  $A'(Z)$  and  $B'(Z)$ , not constants with height. Physically,  $A'(Z)$  and  $B'(Z)$  should strongly correlate with the profiles of cloud and drizzle microphysical properties, more precisely, to  $r_c(Z)$  and  $r_d(Z)$ .

Note that KK scheme is used as an example in this study in which we first calculate  $P_r(Z)$  by summing  $R_{auto}(Z)$  and  $R_{accr}(Z)$ , and then constrain the original  $R_{auto}(Z)$  and  $R_{accr}(Z)$  with retrieved  $LWC_d(Z)$  in Equations 3 and 4. The approaches can only be applied to schemes having both  $R_{auto}$  and  $R_{accr}$  parameterizations, while those having one of them, such as having  $A_{auto}$  in Liu and Daum (2004), cannot be modified in this study.

## 2.2. CESM Simulations

The NSF/DOE CESM version 1.2.2 (Hurrell et al., 2013) is used in this study to access the impacts of altered warm rain microphysics on cloud and precipitation on the regional and global scale. The atmospheric component, Community Atmosphere Model Version 5.3 (CAM5), possesses notable improvements in simulating cloud and precipitation. In particular, a prognostic two-moment stratiform cloud microphysics scheme (Morrison & Gettelman, 2008) was implemented in the CAM5 for the first time. The KK scheme is used for the warm rain process.

Six-year equilibrium present-day forcing simulations (2000–2005) are performed for each microphysical configuration. The first year (2000) is considered as spin-up, and the last five-year results (2001–2005) are analyzed. To assess the probability density function (PDF) of precipitation rates, typically high frequency (e.g., hourly) precipitation output is required. However, it is computationally expensive to store such high-frequency output in a global climate model. In this study, we adopted an in-situ diagnostic method (Wang et al., 2016) to generate precipitation PDFs based on rain rates at each model time step (the hourly time scale) because this method can also facilitate the comparison between GCM simulated and satellite retrieved transient precipitation rates (Aumann et al., 2018).

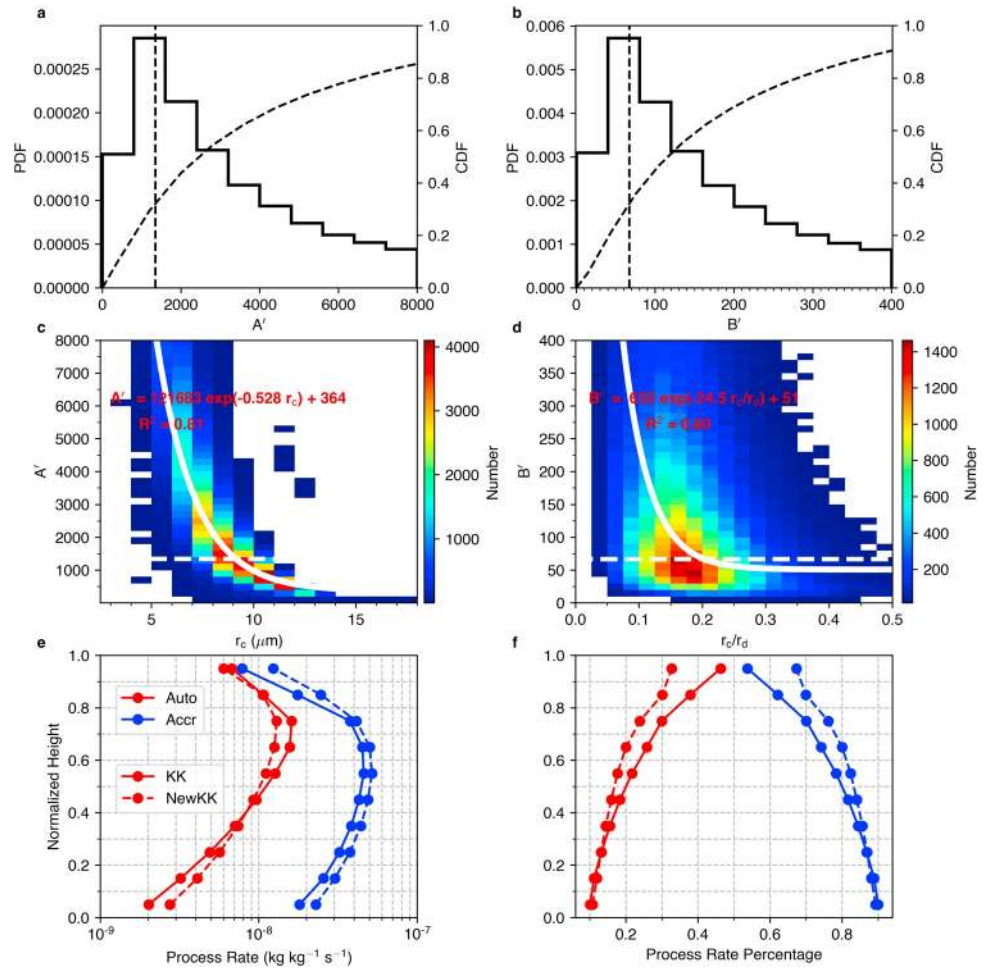


**Figure 1.** (a, b) Probability density functions (PDFs, solid lines) and cumulative density functions (CDFs, dashed curves) of coefficients  $A'(Z)$  and  $B'(Z)$  calculated from ground-based retrievals. Vertical dashed lines mark the constants in the KK scheme. Joint histograms of (c)  $A'(Z)$  with  $r_c(Z)$  and (d)  $B'(Z)$  and the ratio of  $r_c(Z)$  to  $r_d(Z)$ . White solid lines are the exponential fittings. White dashed lines mark the prescribed  $A$  and  $B$  in the KK scheme. (e) Normalized profiles of  $R_{auto}$  (red lines) and  $R_{accr}$  (blue lines) for all the drizzle cases during ACE-ENA (a total 9,213 1-min profiles) by cloud thickness ( $z_i = \frac{z - z_b}{z_t - z_b}$ , where subscripts  $b$  and  $t$  denote cloud base and top, respectively). The solid and dashed lines represent the profiles from KK and NKK schemes, respectively. (f) The percentages of total drizzle water production rate ( $R_{auto} + R_{accr}$ ) contributed by  $R_{auto}$  and  $R_{accr}$ .

### 3. Constrain Cloud Microphysics Scheme Using Ground-based Retrievals

The  $R_{auto}(Z)$  and  $R_{accr}(Z)$  profiles, calculated from ground-based retrievals using Equations 1 and 2, for the case of July 18, 2017 are presented in Figure S2. As expected,  $R_{auto}(Z)$  increases with height, basically follows the  $LWC_c(Z)$  profiles. During drizzle drops falling process,  $R_{accr}(Z)$  becomes increasingly important as demonstrated in Figure S2b where  $R_{accr}(Z)$  is the largest in the cloud center. To recalibrate  $R_{auto}(Z)$  and  $R_{accr}(Z)$  in the KK scheme, we used the retrievals to derive  $A'(Z)$  and  $B'(Z)$  profiles as demonstrated in Figures S2c and S2d. Figures 1a and 1b show the probability density functions (PDFs) and cumulative density functions (CDFs) of  $A'(Z)$  and  $B'(Z)$ . The prescribed  $A$  and  $B$  values (constants) in the KK scheme fall in the same bins as their mode values, suggesting that the prescribed values are representative for the most scenarios.

To be applicable of  $A'(Z)$  and  $B'(Z)$  in model simulations, we parameterized  $A'(Z)$  and  $B'(Z)$  as exponential functions of  $r_c(Z)$  and  $r_c(Z)/r_d(Z)$  in Figures 1c and 1d as:

$$A'(Z) = 121683 \exp(-0.528 r_c(Z)) + 364, \quad (5)$$

$$B'(Z) = 632 \exp\left(-24.5 \frac{r_c(Z)}{r_d(Z)}\right) + 51. \quad (6)$$

The profiles of  $A'(Z)$  and  $B'(Z)$  in Figure S2 are smaller than their prescribed values in the upper part and greater in the lower part of the cloud. The joint PDFs of  $A'(Z)$  and  $r_c(Z)$  with an exponential relationship between them (Equation 5) are illustrated in Figure 1c. We find that  $A'(Z)$  decreases with increasing  $r_c(Z)$  and becomes smaller than the prescribed  $A$  when  $r_c(Z)$  is greater than  $\sim 9 \mu\text{m}$ . Physically,  $R_{\text{auto}}$  should increase with increasing  $r_c(Z)$ , the result here suggests that the power law functions for  $q_c(Z)$  and  $N_c$  in Equation 1 are too strong and the fitted exponential formula  $A'(Z)$  acts to reduce the power law relationship and bring  $R'_{\text{auto}}(Z)$  to more reasonable values to correct the overestimated  $LWC_d(KK)$  in the upper part and underestimated  $LWC_d(KK)$  in the lower part of the cloud as shown in Figure S1f. Introducing  $r_c(Z)$  in Equation 3 adds a more direct constraint on the autoconversion process than the relationship originally used in KK because the autoconversion process is primarily a conversion process from cloud droplets to drizzle drops near the cloud top.

Similarly, we fitted an exponential function between  $B'(Z)$  and  $r_c(Z)/r_d(Z)$  (Equation 6) in Figure 1d.  $B'(Z)$  decreases with increasing  $r_c(Z)/r_d(Z)$  until the ratios reach  $\sim 0.2$ . The fitted formula and the pattern of the joint PDF, as well as Figure S1f, reveal that  $B'(Z)$  values should change with height. Near the cloud top,  $r_c(Z)$  is the largest while  $r_d(Z)$  is the smallest, resulting in the greatest  $r_c(Z)/r_d(Z)$ , where  $B'(Z)$  from the NKK scheme are the smallest and remain nearly constant ( $\sim 50$ ) for  $r_c(Z)/r_d(Z) > 0.2$ , even smaller than the prescribed  $B$  ( $B = 67$ ). From the cloud top to the cloud base,  $r_c(Z)$  decreases but  $r_d(Z)$  increases, resulting in the smallest  $r_c(Z)/r_d(Z)$  at the bottom of the cloud.  $B'(Z)$  increases with decreasing  $r_c(Z)/r_d(Z)$  from the top to the base and reaches the largest value at the bottom of the cloud. This change in  $B'(Z)$  will counterbalance the overestimated  $LWC_d(KK)$  in the upper part and underestimated  $LWC_d(KK)$  in the lower part of the cloud as demonstrated in Figure S1f.

Theoretically, the collision efficiency is the highest and reaches nearly unity for  $r_c(Z)/r_d(Z) > 0.2$ , while the collision efficiency decreases significantly with decreasing  $r_c(Z)/r_d(Z)$  (Rogers & Yau, 1996). With fixed drizzle drop size, larger cloud droplets have higher collision efficiency and correspondingly larger  $R_{\text{auto}}$  values, which typically happens near the cloud top. For smaller cloud droplets, their collision efficiencies are much lower because they tend to follow the streamlines around a falling drizzle drop. However, the coalescence efficiency is opposite to the collision efficiency, that is, smaller cloud droplets more easily stay with drizzle drops and remain joined. This argument is further proved from the retrieved  $r_c(Z)$ ,  $r_d(Z)$ ,  $LWC_c(Z)$  and  $LWC_d(Z)$  in Figure S1 and  $R_{\text{auto}}$  and  $R_{\text{accr}}$  in Figures 1e and 1f.  $R_{\text{auto}}$  contribution to drizzle water content increases with height, peaking near the cloud top which basically follows the  $r_c(Z)$  and  $LWC_c(Z)$  variations, while  $R_{\text{accr}}$  contributes most near the cloud base which is attributed by  $r_d(Z)$  and  $LWC_d(Z)$ .

The fitted exponential formula between  $B'(Z)$  and  $r_c(Z)/r_d(Z)$  in Figure 1d is opposite to the theoretical collision efficiency. This is because the KK scheme tends to overestimate  $LWC_d(KK)$  near the cloud top and  $B'(Z)$  should be decreased in order to lessen  $R_{\text{accr}}$ . Near the cloud base,  $B'(Z)$  is usually the largest from the NKK scheme, which acts to enhance  $R_{\text{accr}}$  to compensate the underestimation of  $LWC_d(KK)$ .

For warm rain processes, cloud droplets normally form at the cloud base, grow with height through condensation in updrafts into the largest cloud droplets ( $r_c \sim 20 \mu\text{m}$ , Rogers & Yau, 1996; Takahashi et al., 2017; Wallace & Hobbs, 2006; Wood, 2005a, 2005b), and become drizzle-sized drops through the collision-coalescence near the cloud top in which  $R_{\text{auto}}$  becomes important (Cheng & Xu, 2009; Liu & Daum, 2004; Wu et al., 2015). These drizzle drops fall from near the cloud top grow by collecting cloud droplets and small drizzle drops. As drizzle drops fall,  $R_{\text{accr}}$  becomes increasingly important.

To quantify the cloud-to-rain particle conversion and growth processes, we normalized the individual profiles in cloud height coordinate.  $R_{\text{auto}}(Z)$  and  $A_{\text{accr}}(Z)$  are calculated from prescribed  $A$  and  $B$  (constants, white dashed lines in Figures 1c and 1d) in the KK scheme, while the NKK scheme  $A'(Z)$  and  $B'(Z)$  are function of  $r_c(Z)$  and  $r_c(Z)/r_d(Z)$  as shown in Figures 1c and 1d (solid while lines). Figure 1e shows the composite

profiles of  $R_{auto}$  and  $R_{accr}$  for all the drizzle cases during ACE-ENA. The normalized  $R_{auto}$  increased significantly with height, with a peak at  $z_i \sim 0.75$ , and then decreased toward the cloud top. The smaller  $R_{auto}$  values at the cloud top are mainly caused by cloud droplet evaporation associated with cloud-top entrainment as observed by aircraft in situ measurements (Wu et al., 2020). The normalized  $R_{accr}$  values are, in general, one order of magnitude greater than the  $R_{auto}$  except at the cloud top where they are closer. The  $R'_{auto}(Z)$  values are slightly less than the  $R_{auto}(Z)$  values in the upper part of the cloud and greater in the lower part. The  $R'_{accr}(Z)$  values, on the other hand, are greater than the  $R_{auto}(Z)$  values at all levels.

The relative contributions of  $R_{auto}$  and  $R_{accr}$  to total drizzle water production rate ( $P_r = A_{auto} + A_{accr}$ ) are presented in Figure 1f.  $R_{auto}(Z)$  and  $R_{accr}(Z)$  contribute  $\sim 45\%$  and  $55\%$  of  $P_r(Z)$  near the cloud top, respectively. As drizzle drops fall,  $R_{accr}$  becomes increasingly important. For the NKK scheme, the  $R'_{auto}(Z)$  and  $R'_{accr}(Z)$  contribute  $\sim 31\%$  and  $\sim 69\%$  of  $P_r(Z)$  near the cloud top, which are 14% less and more, respectively, than the contributions from the KK scheme. The relative contributions of autoconversion (accretion) gradually decrease (increase) toward the cloud base and have nearly the same in both schemes below  $z_i = 0.3$ . Near the cloud top, the 14% lower contribution from  $R'_{auto}(Z)$  corroborates that the NKK scheme has lower precipitation frequency than the KK scheme. On the other hand, the 14% greater contribution from  $R'_{accr}(Z)$  confirms that the NKK scheme has higher precipitation intensity than the KK scheme. At the upper part of the clouds, the less (more) autoconversion (accretion) contributions from the NKK scheme corroborate the notion that the KK scheme overestimated autoconversion rates and underestimated accretion rates, which could be a reason that most GCMs predict “too frequent and too light precipitation.” Meanwhile, the NKK scheme has the potential to mitigate the outstanding problem in GCM precipitation simulations and shed light on future model development.

Notice that the focus of this study is on the vertical distributions of  $R_{auto}$  and  $R_{accr}$ , and their impacts on precipitation simulation. The spatial variations of  $R_{auto}$  and  $R_{accr}$ , especially their subgrid variabilities, should share the equal importance in precipitation simulation. For example, Wu et al. (2018) calculated the so-called enhancement factors,  $E_{auto}$  and  $E_{accr}$ , using ARM ENA ground-based observations and retrievals. They found both enhancement factors increase with the increase of model grid size. These results are similar to those from Xie and Zhang (2015) and results from satellite observations in Lebsock et al. (2013) and Zhang et al. (2019). Comparing the prescribed enhancement factors in Morrison and Gettelman (2008) to the observed ones, a higher  $E_{auto}(3.2)$  and a lower  $E_{accr}(1.07)$  at small grids were used in Morrison and Gettelman (2008). In this study, however, we only investigate the vertical distribution of  $A_{auto}$  and  $A_{accr}$  and their impact on precipitation with prescribed enhancement factors in CESM simulations.

#### 4. Impacts of the Updated Microphysics Scheme in Climate Simulations

The KK scheme has been widely used in cloud-resolving (Seinfeld et al., 2016) and global climate models, including the NCAR/DOE CESM (Gettelman et al., 2019; Hurrell et al., 2013; Morrison & Gettelman, 2008). In this study, we implemented the updated schemes  $R'_{auto}(Z)$  and  $R'_{accr}(Z)$  in CESM version 1.2 (CESM1) to assess the climatic influence of recalibrated cloud microphysical processes. We first compare the standard CESM1 simulations with the satellite products to justify the rationale of updating microphysics scheme. The CERES Edition 4 cloud liquid water path (LWP) retrievals from the Moderate Resolution Imaging Spectroradiometer (MODIS) and shortwave cloud radiative forcing (SWCF) from the Clouds and the Earth's Radiant Energy System (CERES) on board of the Terra and Aqua satellites (Minnis et al., 2020) will serve as the benchmark. Figure 2 shows the CESM1 simulated spatial distributions of maritime LWPs between 60°S and 60°N with a mean of 43.0 g/m<sup>2</sup>, which is close to the satellite retrieval (44.1 g/m<sup>2</sup>). However, large differences exist over some regions. For example, there are positive biases of LWP in CESM1 over the Inter Tropical Convergence Zone, whereas over the stratocumulus-prevailing regions such as the Southeast Pacific and Southeast Atlantic, the negative biases can be up to  $-20$  g/m<sup>2</sup> as shown in Figure 2e, which is consistent with the common problem of GCM, that is too frequent drizzle precipitation for stratus and stratocumulus clouds.

The spatial distributions of observed and modeled SWCF values have strong negative correlations with their corresponding LWPs, that is, larger LWP corresponds to stronger negative SWCF as illustrated in Figures 2b and 2d. The spatial distribution of the biases in SWCF (Figure 2f) mirrors those in LWP (Figure 2e), indi-

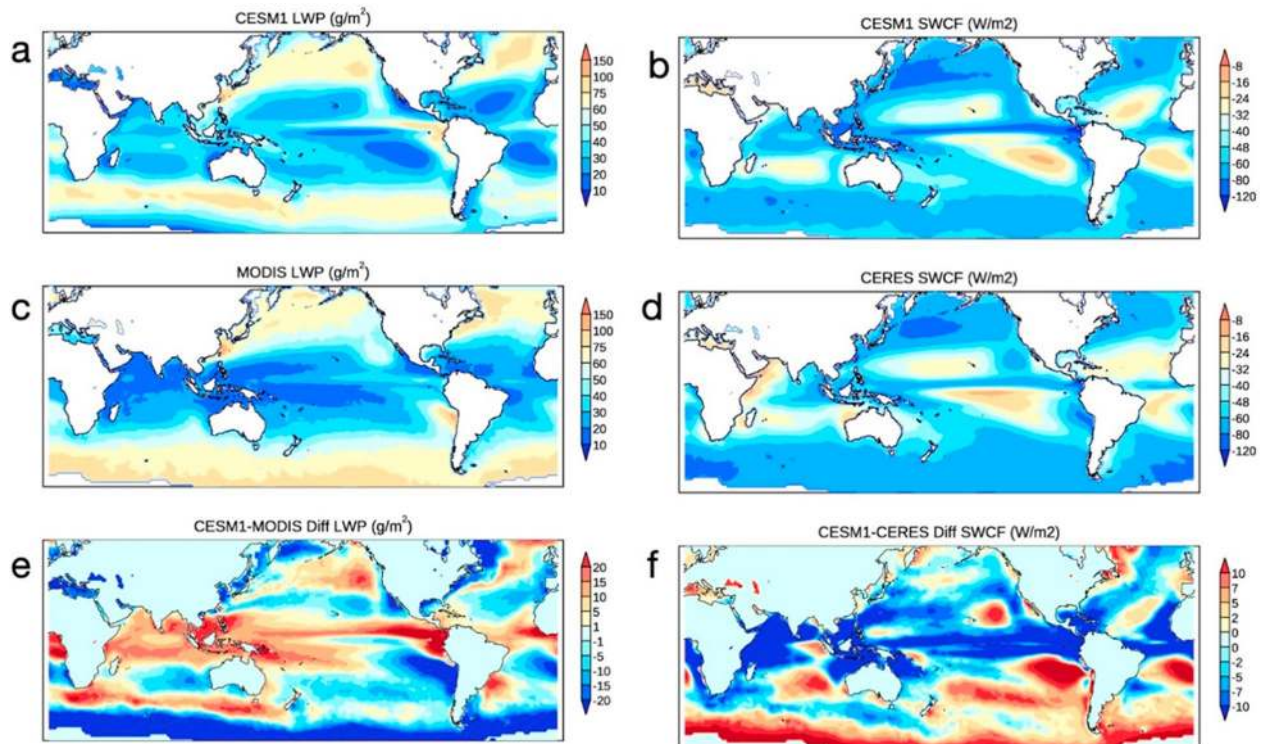


**Figure 2.** Comparisons of cloud liquid water path (LWP, left column) and shortwave cloud forcing (SWCF, right column) between Community Earth System Model (CESM1) present-day scenario simulations (a, b) and CERES-MODIS satellite cloud and radiation climatologies (c,d), as well as their differences (e, f). Model simulations consist of five ensemble members. Satellite data are averaged over 2001–2019 from both Terra and Aqua satellites.

indicating that the SWCF biases are largely contributed by those in LWP. Over  $60^\circ\text{S}$  to  $60^\circ\text{N}$ , the oceanic SWCF bias is  $-2.3\text{ W/m}^2$ . In addition to CESM1 simulations, we also simulate cloud LWP using CESM2 (version 2.1.1) whose microphysical scheme includes an enhancement factor in the KK scheme. However, the LWP in CESM2 is found to be overestimated by 66% in comparison with satellite observations (Figure S3). Therefore, we choose not to test our observational constraints in CESM2.

To reveal the relative importance of the changes in  $R_{\text{auto}}$  and  $R_{\text{accr}}$  parameterizations, we conducted two model sensitivity studies by using  $R'_{\text{auto}}(Z)$  first, and then using both  $R'_{\text{auto}}(Z)$  and  $R'_{\text{accr}}(Z)$  in CESM1. Figure 3a shows the differences in maritime stratiform cloud LWP between the simulations using  $R'_{\text{auto}}(Z)$  and  $R_{\text{auto}}(Z)$  in which  $R'_{\text{auto}}(Z)$  significantly increased cloud LWP. Such an increase is more evident in the mid-latitude regions than the tropics, which can be attributed to the fact that the stratiform clouds are more prevalent in the mid-latitudes. The increased LWPs in the mid-latitudes using NKK greatly counterbalance the negative biases in LWP using KK scheme (Figure 3e), bring the modeled LWPs closer to satellite retrievals. In particular, the simulated LWPs using  $R'_{\text{auto}}(Z)$  increased  $11.8\text{ g m}^{-2}$  over  $60^\circ\text{S}$ – $60^\circ\text{N}$  oceanic regions (Figure 3a) which is more than 20% fractional changes, and  $9.8\text{ g m}^{-2}$  globally (Figure S4b). The increases in mean stratiform cloud fractions (CFs) were only 0.5% and 0.8% for the mid-latitudes and globally (Figure S5), but much more for fractional changes, up to 10% over the regions such as subtropics and the Arctic as seen in Figure S5d.

The reduced  $R'_{\text{auto}}(Z)$  near the cloud top shown in Figure 1f corroborates the notion that the overestimation of  $R_{\text{auto}}$  is more important in determining the overall  $R_{\text{auto}}$  effect than the underestimation of  $R_{\text{auto}}$  in the bottom of the cloud. Hence,  $R'_{\text{auto}}(Z)$  exerts a larger influence on the height dependency of precipitation processes in the cloud. In contrast,  $R_{\text{accr}}$  is generally underestimated throughout the whole cloud profile (Figures 1e and 1f). Therefore, a stronger  $R'_{\text{accr}}(Z)$  can be expected when implementing it in the model simulations, which can result in more cloud LWP as evident in Figure 3a. Taking changes by both  $R'_{\text{auto}}(Z)$  and  $R'_{\text{accr}}(Z)$  into account together, the net cloud LWP changes (Figure 3b) are much less than those simulated with  $R'_{\text{auto}}(Z)$  only in Figure 3a, but are still dominated by the impact of the autoconversion change, with

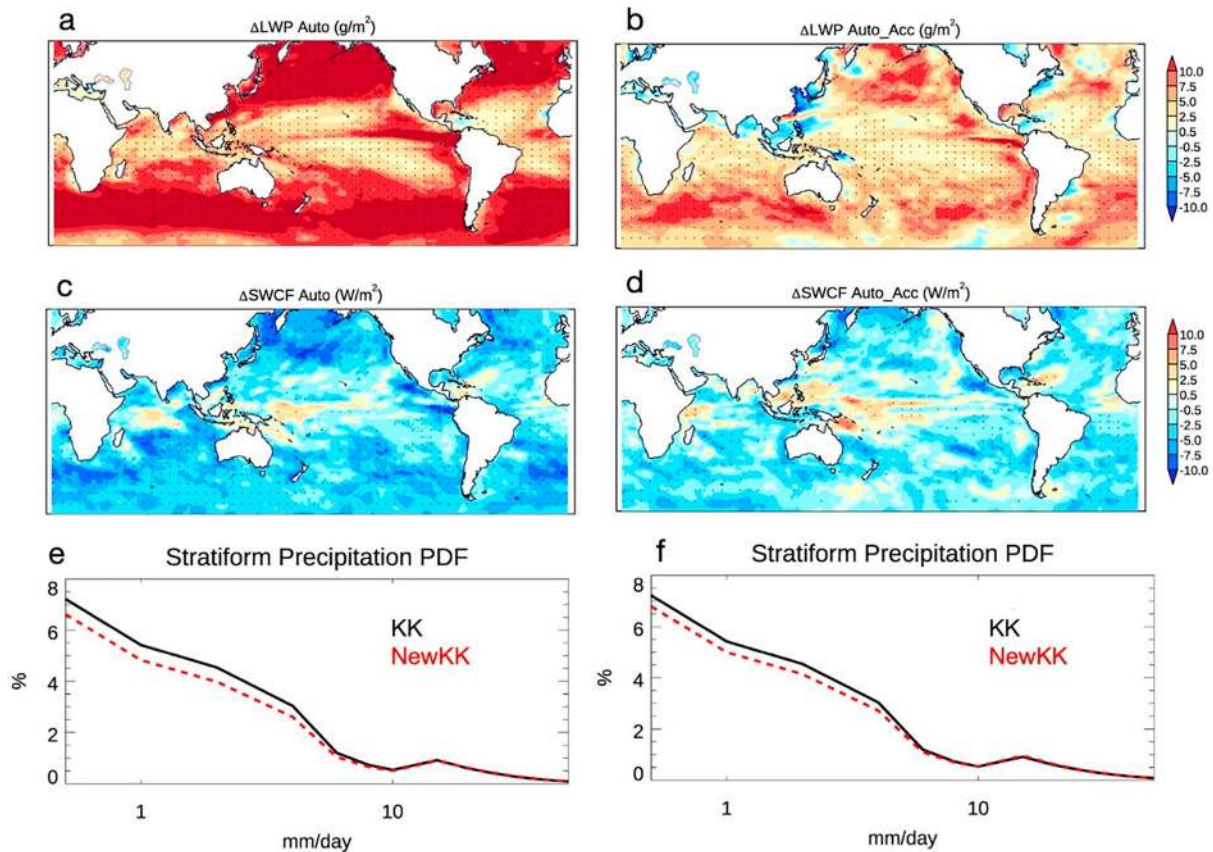


**Figure 3.** Changes in liquid water path (LWP) (a, b), shortwave cloud radiative forcing (SWCF) (c, d), and Probability distribution functions (PDFs) of large-scale stratiform precipitation (e, f) in Community Earth System Model (CESM) simulations by different warm rain schemes (NKK – KK). Left column: autoconversion only. Right column: both autoconversion and accretion. The stippling indicates the statistically significant changes that are larger than the model internal variability (calculated as the standard deviation among the ensemble members). The precipitation PDF are averaged over 60°S to 60°N oceanic regions. The spreads of precipitation frequency in each bin are all less than 0.1% among different ensemble members, so they are too small to be shown in the panels (e) and (f).

a mean increase of  $4.5 \text{ g m}^{-2}$  over 60°S–60°N oceanic regions, corresponding to a 10% increase. No significant changes in stratiform CFs using  $R'_{\text{auto}}(Z)$  only or both  $R'_{\text{auto}}(Z)$  and  $R'_{\text{accr}}(Z)$  are found in this study (Figure S5).

Cloud-to-rain particle conversion is also crucial for drizzle formation process in clouds. With suppressed autoconversion rates near the cloud top, the  $R'_{\text{auto}}(Z)$  results in significant reductions in precipitation frequency, particularly in the subtropical regions (Figures S4c and S4d). Figure S4d illustrates the decreased precipitation frequency corresponded with increased cloud LWP (Figure S4b) and stratiform CF (Figure S5), although they were imperfectly matched in their spatial distributions. Similar to the cloud responses, the rain formation process is dominated by the autoconversion change. This conclusion is further confirmed in Figures S4c and S4d where the mean absolute changes in global precipitation frequency are  $-3.1\%$  with  $R'_{\text{auto}}(Z)$  only and  $-2.6\%$  with both  $R'_{\text{auto}}(Z)$  and  $R'_{\text{accr}}(Z)$ , with a significant decrease over the tropical regions.

To further probe the surface precipitation changes as a function of rain intensity, we employed an in situ diagnostic method (Wang et al., 2016) to generate precipitation PDFs based on rain rates on the hourly time scale. During the model integration, at each model time step, the new diagnostic accumulates instantaneous precipitation rates into 30 predefined bins. At the end of each month, the corresponding percentage for each bin can be calculated to obtain a PDF and output it in the monthly data. The model sensitivity run shows that for the stratiform clouds, the mean frequency of drizzle or light precipitation (intensities less than 5 mm/day) was reduced from 25.2% to 22.7% when  $R'_{\text{accr}}(Z)$  was applied (Figure 3e), corresponding to a 10% fractional decrease. With an elevated accretion rate in the NKK scheme updating both processes, a



7.3% (fractional) drizzle reduction still exists. The reduced precipitation frequency with the NKK scheme alleviates a long-lasting problem related with the precipitation in GCMs (Stephens et al., 2010). It is difficult to obtain stratiform precipitation from observations, so we do not compare the stratiform precipitation PDF with observations in this study. Wang et al. (2016) examined the total precipitation PDF in the CESM1 simulations using the KK scheme, and found that the simulated precipitation frequency for light precipitation frequency is 5% higher than the Tropical Rainfall Measuring Mission (Lau & Wu, 2011) observations (54%) over the tropical region of 25°S–25°N. Although it is not the same region as this study (60°S–60°N), this result corroborates that the simulated precipitation frequency using the NKK scheme is changing toward to observed one.

## 5. Conclusions

It is a great challenge to realistically simulate low clouds and associated warm rain in climate models without reliable vertical variations of microphysical processes. In this work, we use the newly retrieved cloud and drizzle microphysical properties to constrain the autoconversion and accretion parameterizations in a widely used microphysical scheme, and then implement the updated scheme into the NCAR CESM to examine the responses of warm rain frequency and cloud properties. Climate simulations with the updated cloud microphysical scheme exhibit the reduced precipitation frequency and increased precipitation intensity, indicating that the new scheme has the potential of mitigating the outstanding problem in GCM precipitation simulations and achieving more accurate climate assessments.

The findings from this study attest the paramount importance of cloud microphysics parameterizations in GCM simulations. In particular, we show that it is critical to take the in-cloud vertical variations of warm rain processes into account when developing cloud microphysical schemes. We note that the robustness of our findings is subject to the representative of new parameterizations derived from a field campaign. Therefore, it is imperative to use more ground-based observations from different field campaigns and ARM permanent sites as well as a single column modeling framework to test if these new parameterizations are valid over other oceans and land surfaces. Future study will also focus on how altered warm rain processes can influence the aerosol indirect effect, cloud feedback, and climate sensitivity.

## Data Availability Statement

The data can be downloaded from <http://www.archive.arm.gov/>. Ground-based MBL cloud and drizzle microphysical property retrievals are archived at <https://doi.org/10.6084/m9.figshare.13205981.v1>.

## Acknowledgments

This research was supported by the NSF project under grant AGS-1700728/AGS-2031750 at the University of Arizona and AGS-1700727/AGS-2031751 at California Institute of Technology. The researchers at the University of Arizona were also supported as part of the “Enabling Aerosol-cloud interactions at GLOBal convection-permitting scales (EAGLES)” project (74358), funded by the U.S. Department of Energy, Office of Science, Office of Biological and Environmental Research (BER), Earth System Modeling program with the sub-contract to the University of Arizona. Y.W. acknowledges the support of the Jet Propulsion Laboratory, California Institute of Technology, under contract with NASA. Measurements during ACE-ENA IOP were obtained from the Atmospheric Radiation Measurement (ARM) Program sponsored by the U.S. Department of Energy (DOE) Office of Energy Research, Office of Health and Environmental Research, and Environmental Sciences Division.

## References

- Albrecht, B. A. (1989). Aerosols, cloud microphysics, and fractional cloudiness. *Science*, *245*(4923), 1227–1230. <https://doi.org/10.1126/science.245.4923.1227>
- Aumann, H. H., Behrangi, A., & Wang, Y. (2018). Increased frequency of extreme tropical deep convection: AIRS observations and climate model predictions. *Geophysical Research Letters*, *45*, 13530–13537. <https://doi.org/10.1029/2018gl079423>
- Beheng, K. D. (1994). A parameterization of warm cloud microphysical conversion processes. *Atmospheric Research*, *33*, 193–206. [https://doi.org/10.1016/0169-8095\(94\)90020-5](https://doi.org/10.1016/0169-8095(94)90020-5)
- Bony, S., & Dufresne, J. L. (2005). Marine boundary layer clouds at the heart of tropical cloud feedback uncertainties in climate models. *Geophysical Research Letters*, *32*, 1–4. <https://doi.org/10.1029/2005gl023851>
- Cheng, A., & Xu, K.-M. (2009). A PDF-based microphysics parameterization for simulation of drizzling boundary layer clouds. *Journal of the Atmospheric Sciences*, *66*, 2317–2334. <https://doi.org/10.1175/2009jas2944.1>
- Dong, X., Xi, B., Kennedy, A., Minnis, P., & Wood, R. (2014). A 19-month record of marine aerosol-cloud-radiation properties derived from DOE ARM mobile facility deployment at the Azores. Part I: Cloud fraction and single-layered MBL cloud properties. *Journal of Climate*, *27*, 3665–3682. <https://doi.org/10.1175/jcli-d-13-00553.1>
- Dong, X., Xi, B., & Wu, P. (2014). Investigation of the diurnal variation of marine boundary layer cloud microphysical properties at the Azores. *Journal of Climate*, *27*, 8827–8835. <https://doi.org/10.1175/jcli-d-14-00434.1>
- Donner, L. J., Wyman, B. L., Hemler, R. S., Horowitz, L. W., Ming, Y., Zhao, M., et al. (2011). The dynamical core, physical parameterizations, and basic simulation characteristics of the atmospheric component AM3 of the GFDL global coupled model CM3. *Journal of Climate*, *24*, 3484–3519. <https://doi.org/10.1175/2011jcli3955.1>
- Fan, J., Wang, Y., Rosenfeld, D., & Liu, X. (2016). Review of aerosol-cloud interactions: Mechanisms, significance, and challenges. *Journal of the Atmospheric Sciences*, *73*(11), 4221–4252. <https://doi.org/10.1175/jas-d-16-0037.1>
- Gettelman, A., Hannay, C., Bacmeister, J. T., Neale, R. B., Pendergrass, A. G., Danabasoglu, G., et al. (2019). High climate sensitivity in the community Earth system model Version 2 (CESM2). *Geophysical Research Letters*, *46*, 8329–8337. <https://doi.org/10.1029/2019gl083978>

- Ghan, S., Wang, M., Zhang, S., Ferrachat, S., Gettelman, A., Griesfeller, J., et al. (2016). Challenges in constraining anthropogenic aerosol effects on cloud radiative forcing using present-day spatiotemporal variability. *Proceedings of the National Academy of Sciences of the United States of America*, *113*(21), 5804–5811. <https://doi.org/10.1073/pnas.1514036113>
- Golaz, J.-C., Larson, V. E., & Cotton, W. R. (2002). A PDF-based model for boundary layer clouds. Part II: Model results. *Journal of the Atmospheric Sciences*, *59*, 3552–3571. [https://doi.org/10.1175/1520-0469\(2002\)059<3552:apbmf>2.0.CO;2](https://doi.org/10.1175/1520-0469(2002)059<3552:apbmf>2.0.CO;2)
- Hang, Y., L'Ecuyer, T. S., Henderson, D. S., Matus, A. V., & Wang, Z. (2019). Reassessing the effect of cloud type on Earth's energy balance in the age of active space borne observations. Part II: Atmospheric heating. *Journal of Climate*, *32*, 6219–6236. <https://doi.org/10.1175/jcli-d-18-0754.1>
- Hurrell, J. W., Holland, M. M., Gent, P. R., Ghan, S., Kay, J. E., Kushner, P. J., et al. (2013). The community Earth system model: A framework for collaborative research. *Bulletin of the American Meteorological Society*, *94*, 1339–1360. <https://doi.org/10.1175/bams-d-12-00121.1>
- IPCC (2013). *Climate change 2013: The physical science basis. Contribution of Working Group I to the Fifth Assessment Report of the Intergovernmental Panel on Climate Change* [Stocker, T.F., D. Qin, G.-K. Plattner, M. Tignor, S.K. Allen, J. Boschung, A. Nauels, Y. Xia, V. Bex and P.M. Midgley (eds.)]. Cambridge University Press, Cambridge, UK, and New York, NY, USA. <https://doi.org/10.1017/CBO9781107415324>
- Jing, X., & Suzuki, K. (2018). The impact of process-based warm rain constraints on the aerosol indirect effect. *Geophysical Research Letters*, *45*, 10729–10737. <https://doi.org/10.1029/2018gl079956>
- Jing, X., Suzuki, K., Guo, H., Goto, D., Ogura, T., Koshiro, T., & Müllmenstädt, J., et al. (2017). A multimodel study on warm precipitation biases in global models compared to satellite observations. *Journal of Geophysical Research: Atmospheres*, *122*, 11806–11824. <https://doi.org/10.1002/2017jd027310>
- Kay, J. E., L'Ecuyer, T., Pendergrass, A., Chepfer, H., Guzman, R., & Yettella, V. (2018). Scale-aware and definition-aware evaluation of modeled near-surface precipitation frequency using CloudSat observations. *Journal of Geophysical Research: Atmospheres*, *123*, 4294–4309. <https://doi.org/10.1002/2017jd028213>
- Kessler, E. (1969). On the distribution and continuity of water substance in atmospheric circulations. In *Meteorological Monographs* (pp. 10–14). American Meteorological Society. [https://doi.org/10.1007/978-1-935704-36-2\\_1](https://doi.org/10.1007/978-1-935704-36-2_1)
- Khairoutdinov, M., & Kogan, Y. (2000). A new cloud physics parameterization in a large-eddy simulation model of marine stratocumulus. *Monthly Weather Review*, *128*, 229–243. [https://doi.org/10.1175/1520-0493\(2000\)128<0229:ancppi>2.0.CO;2](https://doi.org/10.1175/1520-0493(2000)128<0229:ancppi>2.0.CO;2)
- Lau, K. M., & Wu, H. T. (2011). Climatology and changes in tropical oceanic rainfall characteristics inferred from Tropical Rainfall Measuring Mission (TRMM) data (1998–2009). *Journal of Geophysical Research* *116*, D17111. <https://doi.org/10.1029/2011JD015827>
- Lebsock, M., Morrison, H., & Gettelman, A. (2013). Microphysical implications of cloud-precipitation covariance derived from satellite remote sensing. *Journal of Geophysical Research: Atmospheres*, *118*, 6521–6533. <https://doi.org/10.1002/jgrd.50347>
- L'Ecuyer, T. S., Hang, Y., Matus, A. V., & Wang, Z. (2019). Reassessing the effect of cloud type on Earth's energy balance in the age of active space borne observations. Part I: Top of atmosphere and surface. *Journal of Climate*, *32*, 6197–6217.
- Li, Z. (2020). East Asian study of tropospheric aerosols and impact on regional cloud, precipitation, and climate (EAST-AIRCPC). *Journal of Geophysical Research: Atmospheres*, *124*, 13026–13054. <https://doi.org/10.1029/2019JD030758>
- Liu, Y., & Daum, P. H. (2004). Parameterization of the autoconversion process. Part I: Analytical formulation of the Kessler-type parameterizations. *Journal of the Atmospheric Sciences*, *61*, 1539–1548. [https://doi.org/10.1175/1520-0469\(2004\)061<1539:potapi>2.0.CO;2](https://doi.org/10.1175/1520-0469(2004)061<1539:potapi>2.0.CO;2)
- Liu, Y., Daum, P. H., McGraw, R. L., Miller, M. A., & Niu, S. (2007). Theoretical expression for the autoconversion rate of the cloud droplet number concentration. *Geophysical Research Letters*, *34*, L16821. <https://doi.org/10.1029/2007gl030389>
- Ma, X., Jia, H., Yu, F., & Quaas, J. (2018). Opposite aerosol index-cloud droplet effective radius correlations over major industrial regions and their adjacent oceans. *Geophysical Research Letters*, *45*, 5771–5778. <https://doi.org/10.1029/2018gl077562>
- Minnis, P., Sun-Mack, S., Chen, Y., Chang, F.-L., Yost, C. R., Smith, W. L., et al. (2020). CERES MODIS cloud product retrievals for Edition 4-- Part I: Algorithm changes. *IEEE Transactions on Geoscience and Remote Sensing*, *58*, 1–37. <https://doi.org/10.1109/TGRS.2020.3008866>
- Morrison, H., & Gettelman, A. (2008). A new two-moment bulk stratiform cloud microphysics scheme in the community atmosphere model, Version 3 (CAM3). Part I: Description and numerical tests. *Journal of Climate*, *21*, 3642–3659. <https://doi.org/10.1175/2008jcli2105.1>
- Nakajima, T. Y., Suzuki, K., & Stephens, G. L. (2010). Droplet growth in warm water clouds observed by the a-train. Part I: sensitivity analysis of the MODIS-derived cloud droplet sizes. *Journal of the Atmospheric Sciences*, *67*, 1884–1896. <https://doi.org/10.1175/2009jas3280.1>
- Penner, J. E., Dong, X., & Chen, Y. (2004). Observational evidence of a change in radiative forcing due to the indirect aerosol effect. *Nature*, *427*, 231–234. <https://doi.org/10.1038/nature02234>
- Rogers, R. R., & Yau, M. K. (1996). *Short course in cloud physics* (3rd ed.). Elsevier.
- Schmidt, G. A., Ruedy, R., Hansen, J. E., Aleinov, I., Bell, N., Bauer, M., et al. (2006). Present-day atmospheric simulations using GISS ModelE: Comparison to in situ, satellite, and reanalysis data. *Journal of Climate*, *19*, 153–192. <https://doi.org/10.1175/jcli3612.1>
- Seinfeld, J. H., Bretherton, C., Carslaw, K. S., Coe, H., DeMott, P. J., Dunlea, E. J., et al. (2016). Improving our fundamental understanding of the role of aerosol–cloud interactions in the climate system. *Proceedings of the National Academy of Sciences of the United States of America*, *113*(21), 5781–5790. <https://doi.org/10.1073/pnas.1514043113>
- Soden, B. J., & Vecchi, G. A. (2011). The vertical distribution of cloud feedback in coupled ocean-atmosphere models. *Geophysical Research Letters*, *38*, L12704. <https://doi.org/10.1029/2011gl047632>
- Stephens, G. L. (2005). Cloud feedbacks in the climate system: A critical review. *Journal of Climate*, *18*, 237–273. <https://doi.org/10.1175/jcli-3243.1>
- Stephens, G. L., L'Ecuyer, T., Forbes, R., Gettelman, A., Golaz, J. C., Bodas-Salcedo, A., et al. (2010). Dreary state of precipitation in global models. *Journal of Geophysical Research*, *115*, D24211. <https://doi.org/10.1029/2010jd014532>
- Stephens, G. L., O'Brien, D., Webster, P. J., Pilewski, P., Kato, S., & Li, J.-I. (2015). The albedo of Earth. *Reviews of Geophysics*, *53*, 141–163. <https://doi.org/10.1002/2014rg000449>
- Suzuki, K., Nakajima, T., Nakajima, T. Y., & Stephens, G. L. (2010). Effect of the droplet activation process on microphysical properties of warm clouds. *Environmental Research Letters*, *5*, 024012. <https://doi.org/10.1088/1748-9326/5/2/024012>
- Suzuki, K., Stephens, G., Bodas-Salcedo, A., Wang, M., Golaz, J.-C., Yokohata, T., & Koshiro, T. (2015). Evaluation of the warm rain formation process in global models with satellite observations. *Journal of the Atmospheric Sciences*, *72*, 3996–4014. <https://doi.org/10.1175/jas-d-14-0265.1>
- Suzuki, K., Stephens, G. L., & Lebsock, M. D. (2013). Aerosol effect on the warm rain formation process: Satellite observations and modeling. *Journal of Geophysical Research: Atmospheres*, *118*, 170–184. <https://doi.org/10.1002/jgrd.50043>
- Takahashi, H., Lebsock, M., Suzuki, K., Stephens, G., & Wang, M. (2017). An investigation of microphysics and subgrid-scale variability in warm-rain clouds using the A-Train observations and a multiscale modeling framework. *Journal of Geophysical Research: Atmospheres*, *122*, 7493–7504. <https://doi.org/10.1002/2016jd026404>

- Tripoli, G. J., Cotton, W. R., Tripoli, G. J., & Cotton, W. R. (1980). A Numerical investigation of several factors contributing to the observed variable intensity of deep convection over south Florida. *Journal of Applied Meteorology*, *19*, 1037–1063. [https://doi.org/10.1175/1520-0450\(1980\)019<1037:aniosf>2.0.CO;2](https://doi.org/10.1175/1520-0450(1980)019<1037:aniosf>2.0.CO;2)
- Wallace, J. M., & Hobbs, P. V. (2006). *Atmospheric science: An introductory survey* (2nd ed.). Elsevier. <https://doi.org/10.1016/C2009-0-00034-8>
- Wang, Y., Ma, P.-L., Jiang, J. H., Su, H., & Rasch, P. J. (2016). Toward reconciling the influence of atmospheric aerosols and greenhouse gases on light precipitation changes in eastern China. *Journal of Geophysical Research: Atmospheres*, *121*, 5878–5887. <https://doi.org/10.1002/2016jd024845>
- Wood, R. (2005a). Drizzle in stratiform boundary layer clouds. Part I: Vertical and horizontal structure. *Journal of the Atmospheric Sciences*, *62*, 3011–3033. <https://doi.org/10.1175/jas3529.1>
- Wood, R. (2005b). Drizzle in stratiform boundary layer clouds. Part II: Microphysical aspects. *Journal of the Atmospheric Sciences*, *62*, 3034–3050. <https://doi.org/10.1175/jas3530.1>
- Wood, R. (2012). Stratocumulus clouds. *Monthly Weather Review*, *140*, 2373–2423. <https://doi.org/10.1175/MWR-D-11-00121.1>
- Wood, R., & Hartmann, D. L. (2006). Spatial variability of liquid water path in marine low cloud: The importance of mesoscale cellular convection. *Journal of Climate*, *19*, 1748–1764. <https://doi.org/10.1175/JCLI3702.1>
- Wood, R., Kubar, T. L., & Hartmann, D. L. (2009). Understanding the importance of microphysics and macrophysics for warm rain in marine low clouds. Part II: Heuristic models of rain formation. *Journal of the Atmospheric Sciences*, *66*, 2973–2990. <https://doi.org/10.1175/2009JAS3072.1>
- Wu, P., Dong, X., & Xi, B. (2015). Marine boundary layer drizzle properties and their impact on cloud property retrieval. *Atmospheric Measurement Techniques*, *8*, 3555–3562.
- Wu, P., Dong, X., Xi, B., Tian, J., & Ward, D. M. (2020). Profiles of MBL cloud and drizzle microphysical properties retrieved from ground-based observations and validated by aircraft in situ measurements over the Azores. *Journal of Geophysical Research: Atmospheres*, *125*, e2019JD032205. <https://doi.org/10.1029/2019JD032205>
- Wu, P., Xi, B., Dong, X. (2018). Evaluation of autoconversion and accretion enhancement factors in general circulation model warm-rain parameterizations using ground-based measurements over the Azores. *Atmospheric Chemistry and Physics*, *18*, 17405–17420.
- Xie, X., & Zhang, M. (2015). Scale-aware parameterization of liquid cloud inhomogeneity and its impact on simulated climate in CESM. *Journal of Geophysical Research: Atmosphere*, *120*, 8359–8371. <https://doi.org/10.1002/2015JD023565>
- Yamaguchi, T., Feingold, G., & Kazil, J. (2017). Stratocumulus to cumulus transition by drizzle. *Journal of Advances in Modeling Earth Systems*, *9*, 2333–2349. <https://doi.org/10.1002/2017MS001104>
- Zhang, Z., Song, H., Ma, P. L., Larson, V. E., Wang, M., Dong, X., & Wang, J. (2019). Subgrid variations of the cloud water and droplet number concentration over the tropical ocean: Satellite observations and implications for warm rain simulations in climate models. *Atmospheric Chemistry and Physics*, *19*, 1077–1096.